INCORPORATING BAYESIAN TRANSFER LEARNING INTO PARTICLE FILTER FOR DUAL-TRACKING SYSTEM WITH ASYMMETRIC NOISE INTENSITIES

A PREPRINT

Omar A. Alotaibi, Brian L. Mark, and Mohammad Reza Fasihi *

November 24, 2025

ABSTRACT

Using Bayesian transfer learning, we develop a particle filter approach for tracking a nonlinear dynamical model in a dual-tracking system where intensities of measurement noise for both sensors are asymmetric. The densities for Bayesian transfer learning are approximated with the sum of weighted particles to improve the tracking performance of the primary sensor, which experiences a higher noise intensity compared to the source sensor. We present simulation results that validate the effectiveness of the proposed approach compared to an isolated particle filter and transfer learning applied to the unscented Kalman filter and the cubature Kalman filter. Furthermore, increasing the number of particles shows an improvement in the performance of transfer learning applied to the particle filter with a higher rate compared to the isolated particle filter. However, increasing the number of particles raises computational time per step. Moreover, the performance gain from incorporating Bayesian transfer learning is approximately linearly proportional to the absolute difference value between the noise intensities of the sensors in the dual-tracking system.

Keywords Object tracking, nonlinear model, Bayesian transfer learning, Bayesian transfer filtering, particle filter, sequential importance resampling, unscented Kalman filter, cubature Kalman filter.

1 Introduction

Tracking systems have recently received significant attention due to the growing demand for higher accuracy in various applications such as object tracking, surveillance, navigation, self-driving vehicles, and computer vision. In object tracking applications, observed data from multiple sensors is often combined using various data fusion techniques to improve overall tracking accuracy [2–4]. In scenarios of a dual separated tracking system, where two tracking systems track the same area at the same time, the two tracking systems are typically assumed to experience similar measurement noise intensity. However, this assumption may not always hold true as each tracking system can encounter various environmental conditions in practice.

We consider a scenario of dual tracking systems for tracking a single object, where the fields of view of the two separated tracking systems overlap. One of the dual-tracking systems is referred to as the primary tracking filter, while the other is the source tracking filter. Each of the tracking systems employs a particle filter to track the common object along a nonlinear trajectory. We shall assume that the primary tracking filter's field of view (FOV) encounters higher noise intensity or clutter in its measurements compared to that of the source tracking filter. Our aim is to improve the tracking performance of the primary tracking filter by leveraging knowledge from the source tracking filter using Bayesian transfer learning (BTL).

---

*A preliminary version of this work was presented in [1]. The authors are with the Department of Electrical and Computer Engineering, George Mason University, Fairfax, VA 22030 USA (e-mail: oalotaib@gmu.edu; bmark@gmu.edu; mfasihi4@gmu.edu).

1.1   Motivation

Transfer learning or *knowledge transfer*, a machine learning technique, has recently been introduced into Bayesian models involving multiple tracking systems [5]. This approach is referred to as BTL [6–9]. Transfer learning allows knowledge gained from a source domain to improve the performance of a target domain that has the challenge of performing its own task accurately. BTL has been adopted to model Gaussian process regression with multiple tasks to effectively address the interactions between the source and target tasks [10, 11]. Furthermore, online object tracking has been modeled using BTL to allow the transfer of visual priors into the tracking process framework to improve performance under complex conditions [12].

A real-world scenario for online transfer learning occurs when multiple operators have tracking systems covering the same area of interest. Such systems often have different configurations, preventing them from processing raw observations from other operators. In this case, common variables, which are predicted observations, can be widely adapted worldwide to be transferred between these operators to enhance each other tracking performance. For instance, ships in a complex maritime environment leverage transferred information for the purpose of enhancing their detection and tracking performance using the Detection Tracking Network (DTNet) [13]. Furthermore, autonomous vehicles of different manufacturers can cooperate through vehicle-to-vehicle (V2V) communication in order to improve tracking performance by recursively sharing useful information [14, 15].

BTL has been applied to a pair of Kalman filters with asymmetric noise intensities for tracking an object following a *linear* motion model [16–20]. The incorporation of BTL with a Bayesian filter, referred to as a Bayesian transfer learning filter (BTLF), aims to enhance the estimation performance of the primary tracking filter, whose FOV is affected by severe conditions, by leveraging gained knowledge from the source tracking filter. In the BTLF framework, the primary tracking filter has no access to any realization of the source tracking system except the observation predictor of the source tracking filter according to [16]. BTLF has been previously applied in [21] to track a *nonlinear* motion model using a *local* approximation approach, where the posterior density follows the form of the prior density. In this approach, the predicted observation parameters, i.e., the mean and covariance, obtained from Bayesian filtering using an unscented Kalman filter, were transferred from the source tracking filter to the primary tracking filter. The BTL approach is different from measurement vector fusion (MVF) [22] and distributed estimation filtering methods such as distributed Kalman filtering (DKF) [23–25], in which the source tracking system directly transfers its estimated states or measurements to the primary tracking system. The drawbacks of MVF and DKF relative to the BTLF approach are as follows: (i) higher communication overhead in transferring cluttered observation data, (ii) one time-step delay in the transferred information, and (iii) from a security or privacy perspective, the raw observation data may contain information that the source may not which to disclose.

1.2   Contribution

To the best of our knowledge, there have been no previous applications of *global* approaches, whereby no explicit assumption is made about the form of the posterior density, in the context of BTLF. A popular global approach for nonlinear filtering is the particle filter (PF) with importance resampling [26, 27]. Our main contribution is to approximate BTLF via a PF to track a nonlinear dynamical motion model in a dual-tracking system under asymmetric measurement noise intensities. Our simulation results show that the estimation accuracy performance of the proposed transfer learning particle filter (TL-PF) scheme, which incorporates BTLF with PF, is significantly superior relative to the performance of an isolated PF under the same conditions. Notably, the TL-PF performance increases at a faster rate than the isolated PF as the number of particles increases, which illustrates the higher sensitivity of TL-PF. The main benefit of the proposed TL-PF approach is that it outperforms not only the isolated PF, but also the integration of unscented Kalman filter (UKF) [28] and cubature Kalman filter (CKF) [29] with BTLF, which we refer to as transfer learning unscented Kalman filter (TL-UKF) and transfer learning cubature Kalman filter (TL-CKF) respectively, as recently published in [30, 31]. This demonstrates the advantages of integrating PF with BTLF to achieve higher accuracy for the challenges of nonlinear motion tracking in dual-tracking systems.

1.3   Organization and Notation

The remainder of this article is organized as follows. Section 2 briefly presents the dynamical nonlinear motion model and formulates the problem of tracking an object using a dual-tracking system with a nonlinear model under asymmetric measurement noise intensities. In Section 3, the BTLF framework is applied to a single object tracking in a dual-tracking system. Section 4 develops the TL-PF scheme and provides procedural steps of the proposed algorithm for the source and primary tracking filters. The numerical results of linear and nonlinear scenarios that demonstrate the effectiveness of the proposed scheme compared to the related tracking filters are presented in Section 5. In addition

to numerical results, Section 5 provides the computational time for incorporating BTL framework to tracking filters in comparison to isolated filters. The article outcomes along with suggested future work are concluded in Section 6.

Notation throughout this article: Uppercase and lowercase letters represent scalars, bold lowercase letters denote vectors, and bold uppercase letters are matrices, $(\cdot)^T$ is the transpose operation of a matrix, $(\cdot)^{-1}$ represents the inverse operation of a matrix, and diag$[\cdot]$ denotes the diagonal of a matrix. $\mathbb{N}$, $\mathbb{N}_0$, $\mathbb{R}$, and $\mathbb{R}^+$ denote the sets of natural, natural with zero, real, and positive real numbers, respectively.

2 Dynamic System Model for Object Tracking

2.1 Nonlinear Motion Model

Consider a discrete-time dynamical nonlinear system [32] described in a state-space representation by the following equations:

$$\mathbf{x}_k = f\left(\mathbf{x}_{k-1}\right) + \mathbf{v}_{k-1}, \tag{1}$$

$$\mathbf{z}_k = h\left(\mathbf{x}_k\right) + \mathbf{w}_k, \tag{2}$$

where $k \in \mathbb{N}_0$ denotes the time step of the discrete-time dynamical system. The state of the system at time k is represented by $\mathbf{x}_k \in \mathbb{R}^{n_\mathsf{x}}$ and $f : \mathbb{R}^{n_\mathsf{x}} \to \mathbb{R}^{n_\mathsf{x}}$ is a nonlinear state transition function. The measurement of the system observed at time k is denoted by a vector $\mathbf{z}_k \in \mathbb{R}^{n_\mathsf{z}}$, which is determined by a nonlinear function $h : \mathbb{R}^{n_\mathsf{x}} \to \mathbb{R}^{n_\mathsf{z}}$ of the state vector. The vectors $\mathbf{v}_{k-1} \in \mathbb{R}^{n_\mathsf{x}}$ and $\mathbf{w}_k \in \mathbb{R}^{n_\mathsf{z}}$ define the process and measurement noises characterizing the uncertainty in the dynamical system. The state $\mathbf{x}_k$ and measurement $\mathbf{z}_k$ vectors for a particular object tracking scenario are defined in Section 5.

2.2 Dual-tracking System with Asymmetric Noise Intensities

We consider a dual-tracking system tracking a single object following the nonlinear motion model provided in (1). The process noise of both sensors is assumed to be independent and identically distributed (i.i.d.) zero-mean Gaussian vector, expressed as $\mathbf{v}_{k-1} \overset{\text{iid}}{\sim} \mathcal{N}(\mathbf{0}, \mathbf{Q_v})$, with the same corresponding covariance $\mathbf{Q_v} \in \mathbb{R}^{n_\mathsf{x} \times n_\mathsf{x}}$ for the source and the primary tracking filters. The two tracking systems track the desired object under the same type of measurement noise, which is assumed to be Gaussian. However, the environmental and surrounding conditions according to the location of each tracking system and its FOV are not necessarily the same. This variation in conditions leads to dissimilar measurement noise intensity that each tracking system experiences. For instance, two self-driving vehicles driving close to each other in the same area where each may be built by a different manufacturer. As shown in Fig. 1, the source tracking system measurements are denoted by $\mathbf{z}_k^\star$ with superscript $\star$, while the primary tracking system measurements are denoted by $\mathbf{z}_k$.

The measurement model represented in (2) will be separated for the source and primary tracking systems, respectively, as

$$\mathbf{z}_k^\star = h\left(\mathbf{x}_k\right) + \mathbf{w}_k^\star, \tag{3}$$

$$\mathbf{z}_k = h\left(\mathbf{x}_k\right) + \mathbf{w}_k, \tag{4}$$

where the measurement noises of the source and primary tracking systems are assumed to be i.i.d. zero-mean Gaussian, i.e.,

$$\mathbf{w}_k^\star \overset{\text{iid}}{\sim} \mathcal{N}(\mathbf{0}, \mathbf{Q_w^\star}) \quad \text{and} \quad \mathbf{w}_k \overset{\text{iid}}{\sim} \mathcal{N}(\mathbf{0}, \mathbf{Q_w}), \tag{5}$$

respectively. The noise covariances of the measurement model are given by $\mathbf{Q_w^\star} = I_\mathbf{w}^\star \mathbf{B_w}$ and $\mathbf{Q_w} = I_\mathbf{w} \mathbf{B_w}$, where $\mathbf{B_w} \in \mathbb{R}^{n_\mathsf{z} \times n_\mathsf{z}}$ is a common diagonal matrix. The noise intensities of the source, $I_\mathbf{w}^\star \in \mathbb{R}^+$, and primary, $I_\mathbf{w} \in \mathbb{R}^+$, tracking systems are assumed to be asymmetric, i.e., $I_\mathbf{w} > I_\mathbf{w}^\star$, (see Section 5 for more definitions and details). The higher level of noise intensity at the primary sensor negatively impacts the reliability of its measurements and its tracking performance. Even though both tracking systems track the same object, their state estimations differ from each other due to the estimation process of each tracking filter conditioning on different observed measurement, with various noise intensity. This yields two estimated states where each tracking filter has its own state estimation. The source tracking filter estimation is denoted by $\mathbf{x}_k^\star$, while the primary tracking filter has an estimated state as $\mathbf{x}_k$

3 Bayesian Transfer Learning Filter Approach

We briefly review the BTLF framework, which was applied in [21, 30] in the context of a dual-tracking system based on the unscented Kalman filter. This framework builds on the concept of shared knowledge introduced in [11, 16]
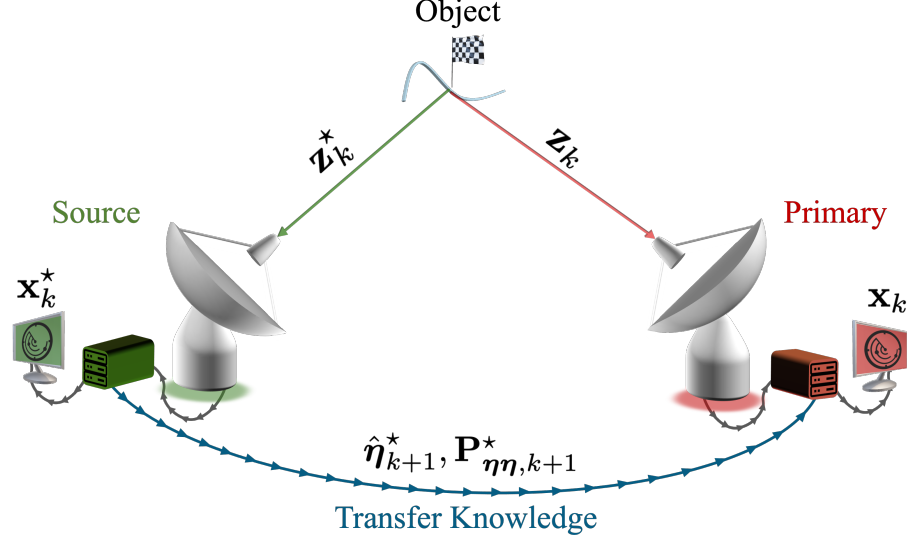
Figure 1: Visualization of a dual-tracking system with asymmetric noise intensities, illustrating the integration of transfer learning.

as refereed to fully probabilistic design (FPD), where the primary tracking filter is able to access the probabilistic parameters by transferring the predicted observation parameters, specifically mean $\hat{\eta}_{k+1}^\star$ and covariance $\mathbf{P}_{\eta\eta,k+1}^\star$, from the source tracking filter.

3.1   Source Tracking Filter

In the source tracking filter, an unknown object state, denoted as $\mathbf{x}_k^\star$, of the current time step k and a predicted observation $\boldsymbol{\eta}_{k+1}^\star$ of the next time step $k+1$ are estimated given a set of observed measurements up to time step k, defined as $\mathbf{z}_{1:k}^\star = \{\mathbf{z}_1^\star, \mathbf{z}_2^\star, \ldots, \mathbf{z}_k^\star\}$. The overall posterior density of the object state and predicted observation $p(\mathbf{x}_k^\star, \boldsymbol{\eta}_{k+1}^\star \mid \mathbf{z}_{1:k}^\star)$ is estimated via two posterior densities as (see [30])

$$p(\mathbf{x}_k^\star, \boldsymbol{\eta}_{k+1}^\star \mid \mathbf{z}_{1:k}^\star) \propto p(\mathbf{x}_k^\star \mid \mathbf{z}_{1:k}^\star) \, p(\boldsymbol{\eta}_{k+1}^\star \mid \mathbf{z}_{1:k}^\star), \tag{6}$$

where the object state posterior and predicted observation densities are expressed, respectively, as

$$p(\mathbf{x}_k^\star \mid \mathbf{z}_{1:k}^\star) \propto p(\mathbf{z}_k^\star \mid \mathbf{x}_k^\star) \, p(\mathbf{x}_k^\star \mid \mathbf{x}_{k-1}^\star) \, p(\mathbf{x}_{k-1}^\star \mid \mathbf{z}_{1:k-1}^\star), \tag{7}$$

and

$$p(\boldsymbol{\eta}_{k+1}^\star \mid \mathbf{z}_{1:k}^\star) \propto p(\boldsymbol{\eta}_{k+1}^\star \mid \mathbf{x}_{k+1}^\star) \, p(\mathbf{x}_{k+1}^\star \mid \mathbf{x}_k^\star) \, p(\mathbf{x}_k^\star \mid \mathbf{z}_{1:k}^\star). \tag{8}$$

The parameter of the predicted observation density in (8) along with the predicted observations are transferred to the primary tracking filter and leveraged in the tracking filter of the next time step to improve tracking accuracy.

3.2   Primary Tracking Filter

The primary tracking filter receives predicted observations up to time step k from the source tracking filter. Given the set of transferred predicted observations $\boldsymbol{\eta}_{2:k}^\star$ and observed measurements up to time step k, the object state posterior density is estimated as (see [30])

$$p(\mathbf{x}_k \mid \mathbf{z}_{1:k}, \boldsymbol{\eta}_{2:k}^\star) \propto p(\mathbf{z}_k \mid \mathbf{x}_k) \, p(\boldsymbol{\eta}_k^\star \mid \mathbf{x}_k) \, p(\mathbf{x}_k \mid \mathbf{x}_{k-1}). \tag{9}$$

Via (9), the state density is estimated by incorporating transferred predicted observations from the source tracking filter as prior knowledge. This yields superior performance for the primary sensor, which has less reliable measurements.

4   Transfer Learning for Particle Filters

We now develop a global approximation approach that integrates particle filtering with a BTLF to approximate posterior densities of the source and primary tracking filters and to leverage the knowledge transferred between tracking

filters. In this section, sequential importance resampling particle filter (SIR-PF) is considered to be the global approach to approximate, which offers improved estimation accuracy compared to local approaches by relaxing assumptions on the forms of prior and posterior densities.

4.1 Source Tracking Filter

The object state posterior density $p(\mathbf{x}_k^\star \mid \mathbf{z}_{1:k}^\star)$ in (7) is approximated using PF with N_s weighted particles given by

$$p(\mathbf{x}_k^\star \mid \mathbf{z}_{1:k}^\star) \approx \sum_{i=1}^{N_s} w_k^{\star(i)} \delta\left(\mathbf{x}_k^\star - \mathbf{x}_k^{\star(i)}\right), \tag{10}$$

where $\delta(\cdot)$ is the Dirac delta function. Ideally, the particles in (10) are sampled directly from the posterior density. Since sampling from the posterior density itself is not possible in most practical scenarios, weighted particles are simply drawn indirectly from a proposal density, which is known as the importance density and derived in Appendix A, defined as

$$\mathbf{x}_k^{\star(i)} \sim q(\mathbf{x}_k^{\star(i)} \mid \mathbf{x}_{k-1}^{\star(i)}, \mathbf{z}_{1:k}^\star)\bigg|_{i=1,\dots,N_s}. \tag{11}$$

The importance density $q(\mathbf{x}_k^{\star(i)} \mid \mathbf{x}_{k-1}^{\star(i)}, \mathbf{z}_{1:k}^\star)$ is chosen to be the state transition prior $p(\mathbf{x}_k^{\star(i)} \mid \mathbf{x}_{k-1}^{\star(i)})$ given in (1). This choice of proposal density was used in [33, 34] to simplify the implementation of the PF. According to this common choice of proposal density, the computation time for sampling from the proposal importance density will be eliminated by propagating samples of the previous time step through the transition model function. After choosing the importance density as the state transition prior, the non-normalized weights in (10) and sampled particles in (11) can be obtained, respectively, as

$$w_k^{\star(i)} \propto w_{k-1}^{\star(i)} \, p(\mathbf{z}_k^\star \mid \mathbf{x}_k^{\star(i)}), \tag{12}$$

and

$$\mathbf{x}_k^{\star(i)} \sim p(\mathbf{x}_k^{\star(i)} \mid \mathbf{x}_{k-1}^{\star(i)})\bigg|_{i=1,\dots,N_s}. \tag{13}$$

Under the assumption $\mathbf{w}_k^\star \overset{\text{iid}}{\sim} \mathcal{N}(\mathbf{0}, \mathbf{Q}_\mathbf{w}^\star)$, the measurement likelihood is utilized to update non-normalized weights in (12) via

$$p(\mathbf{z}_k^\star \mid \mathbf{x}_k^{\star(i)}) = \frac{1}{(2\pi)^{n_\mathbf{z}/2} \sqrt{|\mathbf{Q}_\mathbf{w}^\star|}} \, \exp\left(\rho^{\star(i)}\right), \tag{14}$$

where

$$\rho^{\star(i)} = -\frac{1}{2}\left(\mathbf{z}_k^\star - h(\mathbf{x}_k^{\star(i)})\right)^T (\mathbf{Q}_\mathbf{w}^\star)^{-1} \left(\mathbf{z}_k^\star - h(\mathbf{x}_k^{\star(i)})\right), \tag{15}$$

$\mathbf{z}_k^\star \in \mathbb{R}^{n_\mathbf{z}}$, and $\mathbf{Q}_\mathbf{w}^\star$ is the covariance of the Gaussian measurement noise in (2). The updated weights in (12) are normalized via

$$\tilde{w}_k^{\star(i)} = \frac{w_k^{\star(i)}}{\sum_{i=1}^{N_s} w_k^{\star(i)}}. \tag{16}$$

The resampling step reduces the effect of the degeneracy phenomenon described in [35], which appears after performing the sequential algorithm for a certain number of iterations. This phenomenon causes most particles to receive near-zero weight, rendering them ineffective in the approximation process for the posterior density. This method measures the degeneracy at each time step by computing the effective number of particles N_{eff}, as defined in [33], and plays an important role once the effective number of particles drops below a certain threshold. The systematic resampling technique introduced in [36] is performed at every time step in the Sequential Importance Resampling (SIR) by neglecting particles with low weights and duplicating the higher weighted particles. The new set of particles is re-weighted uniformly by assigning a new weight $w_k^{\star(i)} = 1/N_s$ to each particle as a part of the SIR process.

The state posterior density, $p(\mathbf{x}_k^\star \mid \mathbf{z}_{1:k}^\star) = \mathcal{N}(\mathbf{x}_k^\star; \hat{\mathbf{x}}_k^\star, \mathbf{P}_k^\star)$, is approximately estimated based on the re-sampled particles and new assigned weights with mean $\hat{\mathbf{x}}_k^\star$ computed as

$$\hat{\mathbf{x}}_k^\star = \frac{1}{N_s} \sum_{i=1}^{N_s} \mathbf{x}_k^{\star(i)}, \tag{17}$$

and the associated covariance $\mathbf{P}_k^\star$ is obtained via

$$\mathbf{P}_k^\star = \frac{1}{N_s} \sum_{i=1}^{N_s} \left(\mathbf{x}_k^{\star(i)} - \hat{\mathbf{x}}_k^\star \right) \left(\mathbf{x}_k^{\star(i)} - \hat{\mathbf{x}}_k^\star \right)^T + \mathbf{Q}_{\mathbf{v}}^\star. \tag{18}$$

The predicted observation posterior density $p(\boldsymbol{\eta}_{k+1}^\star \mid \mathbf{z}_{1:k}^\star)$ in (8) is approximated similarly with a set of weighted particles via

$$p(\boldsymbol{\eta}_{k+1}^\star \mid \mathbf{z}_{1:k}^\star) \approx \sum_{i=1}^{N_s} w_{k+1}^{\star\boldsymbol{\eta}(i)} \delta\left(\boldsymbol{\eta}_{k+1}^\star - \boldsymbol{\eta}_{k+1}^{\star(i)}\right), \tag{19}$$

where the importance density $q(\boldsymbol{\eta}_{k+1}^{\star(i)} \mid \mathbf{x}_k^{\star(i)}, \mathbf{z}_{1:k}^\star)$, a proof of derivation is provided in Appendix A, is chosen to be $p(\boldsymbol{\eta}_{k+1}^{\star(i)} \mid \mathbf{x}_k^{\star(i)})$ given as

$$p(\boldsymbol{\eta}_{k+1}^{\star(i)} \mid \mathbf{x}_k^{\star(i)}) = p(\boldsymbol{\eta}_{k+1}^{\star(i)} \mid \mathbf{x}_{k+1}^{\star(i)}) \, p(\mathbf{x}_{k+1}^{\star(i)} \mid \mathbf{x}_k^{\star(i)}). \tag{20}$$

According to the choice of importance density in (20), particles are drawn and weighted as following:

$$\mathbf{x}_{k+1}^{\star(i)} \sim p(\mathbf{x}_{k+1}^{\star(i)} \mid \mathbf{x}_k^{\star(i)})\Big|_{i=1,\ldots,N_s}, \tag{21}$$

$$\boldsymbol{\eta}_{k+1}^{\star(i)} \sim p(\boldsymbol{\eta}_{k+1}^{\star(i)} \mid \mathbf{x}_{k+1}^{\star(i)})\Big|_{i=1,\ldots,N_s}, \tag{22}$$

and

$$w_{k+1}^{\star\boldsymbol{\eta}(i)} = w_k^{\star(i)} = 1/N_s. \tag{23}$$

The mean and covariance for the predicted observation posterior density in (19), which follows a Gaussian model expressed as $p(\boldsymbol{\eta}_{k+1}^\star \mid \mathbf{z}_{1:k}^\star) = \mathcal{N}(\boldsymbol{\eta}_{k+1}^\star; \hat{\boldsymbol{\eta}}_{k+1}^\star, \mathbf{P}_{\boldsymbol{\eta}\boldsymbol{\eta},k+1}^\star)$, are estimated via uniformly weighted sampled particles and computed according to the following expressions:

$$\hat{\boldsymbol{\eta}}_{k+1}^\star = \frac{1}{N_s} \sum_{i=1}^{N_s} \boldsymbol{\eta}_{k+1}^{\star(i)}, \tag{24}$$

$$\mathbf{P}_{\boldsymbol{\eta}\boldsymbol{\eta},k+1}^\star = \frac{1}{N_s} \sum_{i=1}^{N_s} \left(\boldsymbol{\eta}_{k+1}^{\star(i)} - \hat{\boldsymbol{\eta}}_{k+1}^\star\right) \left(\boldsymbol{\eta}_{k+1}^{\star(i)} - \hat{\boldsymbol{\eta}}_{k+1}^\star\right)^T + \mathbf{Q}_{\mathbf{w}}^\star. \tag{25}$$

Note that the estimated mean $\hat{\boldsymbol{\eta}}_{k+1}^\star$ and covariance $\mathbf{P}_{\boldsymbol{\eta}\boldsymbol{\eta},k+1}^\star$ in (24) and (25), respectively, are transferred simultaneously to the primary tracking filter. These transferred parameters, which characterize the predicted observation density in (8), provide valuable knowledge to be leveraged in the estimation process of the primary tracking filter to enhance its tracking performance. The proposed source tracking filter approach is summarized with procedural steps in Algorithm 1.

4.2 Primary Tracking Filter

The primary sensor utilizes the transferred mean and covariance of the predicted observation density from the source tracking filter as a prior to estimate the overall posterior density $p(\mathbf{x}_k \mid \mathbf{z}_{1:k}, \boldsymbol{\eta}_{2:k}^\star)$ given in (9). Using the PF approach, the approximation of the overall posterior density via weighted particles is expressed as

$$p(\mathbf{x}_k \mid \mathbf{z}_{1:k}, \boldsymbol{\eta}_{2:k}^\star) \approx \sum_{i=1}^{N_s} w_k^{(i)} \delta\left(\mathbf{x}_k - \mathbf{x}_k^{(i)}\right), \tag{26}$$

where the particles in (26) are drawn from an importance density, which is derived in Appendix A, as follows:

$$\mathbf{x}_k^{(i)} \sim q(\mathbf{x}_k^{(i)} \mid \mathbf{x}_{k-1}^{(i)}, \mathbf{z}_{1:k}, \boldsymbol{\eta}_{2:k}^\star)\Big|_{i=1,\ldots,N_s}. \tag{27}$$

Algorithm 1 TL-PF Source Tracking Algorithm

Input: $\mathbf{z}_k^\star, \mathbf{x}_k^{\star(i)}, i = 1, \ldots, N_s$
Output: $\hat{\mathbf{x}}_k^\star, \hat{\boldsymbol{\eta}}_{k+1}^\star, \mathbf{P}_{\boldsymbol{\eta\eta},k+1}^\star, \mathbf{x}_{k+1}^{\star(i)}, i = 1, \ldots, N_s$

1: **for** particles, $i \leftarrow 1$ to N_s **do**
2:   Obtain measurement likelihood $p(\mathbf{z}_k^\star \mid \mathbf{x}_k^{\star(i)})$ ▷ (14)
3:   Compute weight $w_k^{\star(i)}$ ▷ (12)
4: **end for**

5: Normalize weights $\tilde{w}_k^{\star(i)} = \frac{w_k^{\star(i)}}{\sum_{i=1}^{N_s} w_k^{\star(i)}}$

6: $\left\{ \mathbf{x}_k^{\star(i)}, w_k^{\star(i)} \right\} =$ Resample $\left\{ \mathbf{x}_k^{\star(i)}, \tilde{w}_k^{\star(i)} \right\}, i = 1, \ldots, N_s$

7: Compute state posterior $p(\mathbf{x}_k^\star \mid \mathbf{z}_{1:k}^\star)$ ▷ (17), (18)

8: **for** particles, $i \leftarrow 1$ to N_s **do**
9:   Draw predicted state particle $\mathbf{x}_{k+1}^{\star(i)}$ ▷ (21)
10:   Draw predicted observation particle $\boldsymbol{\eta}_{k+1}^{\star(i)}$ ▷ (22)
11:   Compute associated weight $w_{k+1}^{\star\boldsymbol{\eta}(i)}$ ▷ (23)
12: **end for**

13: Compute predicted observation posterior
   $p(\boldsymbol{\eta}_{k+1}^\star \mid \mathbf{z}_{1:k}^\star)$ ▷ (24), (25)

Transfer: the estimated density parameters $\hat{\boldsymbol{\eta}}_{k+1}^\star$ and $\mathbf{P}_{\boldsymbol{\eta\eta},k+1}^\star$ to the primary tracking filter.

By choosing the proposal density to be the state transition prior, i.e., $q(\mathbf{x}_k^{(i)} \mid \mathbf{x}_{k-1}^{(i)}, \mathbf{z}_{1:k}, \boldsymbol{\eta}_{2:k}^\star) = p(\mathbf{x}_k^{(i)} \mid \mathbf{x}_{k-1}^{(i)})$, the non-normalized weights in (26) are computed via

$$w_k^{(i)} \propto w_k^{\boldsymbol{\eta}(i)} \, p(\mathbf{z}_k \mid \mathbf{x}_k^{(i)}), \tag{28}$$

where the transferred predicted observation weights are denoted by $w_k^{\boldsymbol{\eta}(i)}$ and defined as

$$w_k^{\boldsymbol{\eta}(i)} \propto w_{k-1}^{(i)} \, p(\boldsymbol{\eta}_k^\star \mid \mathbf{x}_k^{(i)}), \tag{29}$$

and particles that approximate the overall posterior density, formulated in (27), are sampled based on the chosen proposal density as

$$\mathbf{x}_k^{(i)} \sim p(\mathbf{x}_k^{(i)} \mid \mathbf{x}_{k-1}^{(i)}) \Big|_{i=1,\ldots,N_s}. \tag{30}$$

The non-normalized weights are updated using two likelihoods to incorporate the most recent observed measurement and the simultaneously transferred parameters at each time step. The transferred predicted observation weights in (29) are obtained as an initial stage for updating the overall weights in (28) by applying the transferred predicted observation likelihood $p(\boldsymbol{\eta}_k^\star \mid \mathbf{x}_k^{(i)})$, which is given by

$$p(\boldsymbol{\eta}_k^\star \mid \mathbf{x}_k^{(i)}) = \frac{1}{(2\pi)^{n_{\mathbf{z}}/2} \sqrt{|\mathbf{P}_{\boldsymbol{\eta\eta},k}^\star|}} \, \exp\left(\rho^{\boldsymbol{\eta}(i)} \right), \tag{31}$$

where

$$\rho^{\boldsymbol{\eta}(i)} = -\frac{1}{2} \left(\hat{\boldsymbol{\eta}}_k^\star - h(\mathbf{x}_k^{(i)}) \right)^T (\mathbf{P}_{\boldsymbol{\eta\eta},k}^\star)^{-1} \left(\hat{\boldsymbol{\eta}}_k^\star - h(\mathbf{x}_k^{(i)}) \right). \tag{32}$$

After updating the weights through the transferred predicted observation likelihood, the measurement likelihood $p(\mathbf{z}_k \mid \mathbf{x}_k^{(i)})$ is employed to compute the weights in (28). The measurement likelihood is given by

$$p(\mathbf{z}_k \mid \mathbf{x}_k^{(i)}) = \frac{1}{(2\pi)^{n_\mathbf{z}/2} \sqrt{|\mathbf{Q_w}|}} \exp\left(\rho^{(i)}\right), \tag{33}$$

where

$$\rho^{(i)} = -\frac{1}{2} \left(\mathbf{z}_k - h(\mathbf{x}_k^{(i)})\right)^T (\mathbf{Q_w})^{-1} \left(\mathbf{z}_k - h(\mathbf{x}_k^{(i)})\right). \tag{34}$$

The above likelihoods, expressed in (31) and (33), are formulated under the assumption of the measurement model given by (2). Unlike the isolated PF algorithm, TL-PF updates particle weights using transferred density parameters. These include the mean $\hat{\boldsymbol{\eta}}_k^\star$ and its associated covariance $\mathbf{P}_{\boldsymbol{\eta\eta},k}^\star$, which are estimated at the previous time step $k-1$ from the source tracking filter as an additive step introduced mainly for incorporating transferred parameters within the process of the PF framework in addition to the updating step in (33) and (34) via newly observed measurement $\mathbf{z}_k$ with its covariance $\mathbf{Q_w}$. The overall weights associated with each individual particle in (28) are normalized by

$$\tilde{w}_k^{(i)} = \frac{w_k^{(i)}}{\sum_{i=1}^{N_s} w_k^{(i)}}. \tag{35}$$

Similar to the source tracking filter, drawn particles along with their normalized weights are resampled using the systematic resampling technique to mitigate the degeneracy phenomenon effect where the resultant weights are identically equal to $1/N_s$. The overall state posterior density in (26) is modeled as a Gaussian density, expressed as $p(\mathbf{x}_k \mid \mathbf{z}_{1:k}, \boldsymbol{\eta}_{2:k}^\star) = \mathcal{N}(\mathbf{x}_k; \hat{\mathbf{x}}_k, \mathbf{P}_k)$. The mean $\hat{\mathbf{x}}_k$ and associated covariance $\mathbf{P}_k$ of this posterior density are estimated using N_s resampled particles as follows:

$$\hat{\mathbf{x}}_k = \frac{1}{N_s} \sum_{i=1}^{N_s} \mathbf{x}_k^{(i)}, \tag{36}$$

$$\mathbf{P}_k = \frac{1}{N_s} \sum_{i=1}^{N_s} \left(\mathbf{x}_k^{(i)} - \hat{\mathbf{x}}_k\right)\left(\mathbf{x}_k^{(i)} - \hat{\mathbf{x}}_k\right)^T + \mathbf{Q_v}. \tag{37}$$

Algorithm 2 provides detailed steps of the proposed primary tracking filter. The TL-PF algorithm describes an implementation for approximating the BTLF using the PF specifically SIR method by leveraging transferred knowledge from the source tracking filter into the primary tracking filter.

5   Simulation Results

5.1   Scenario 1: Linear Motion Model

5.1.1   Tracking System Model and Parameters Settings

In Scenario 1, we consider a single object following a linear motion model described as

$$\mathbf{x}_k = \begin{bmatrix} 1 & T_s & 0 & 0 \\ 0 & 1 & 0 & 0 \\ 0 & 0 & 1 & T_s \\ 0 & 0 & 0 & 1 \end{bmatrix} \mathbf{x}_{k-1} + \mathbf{v}_{k-1}, \tag{38}$$

where the unknown object state is defined as $\mathbf{x}_k = [x_k, \dot{x}_k, y_k, \dot{y}_k]^T$ consisting of the object's position and velocity denoted by (x_k, y_k) and $(\dot{x}_k, \dot{y}_k)$, respectively. The process noise is a zero-mean Gaussian noise with covariance given by

$$\mathbf{Q_v} = \begin{bmatrix} q\frac{T_s^4}{4} & q\frac{T_s^3}{2} & 0 & 0 \\ q\frac{T_s^3}{2} & qT_s^2 & 0 & 0 \\ 0 & 0 & q\frac{T_s^4}{4} & q\frac{T_s^3}{2} \\ 0 & 0 & q\frac{T_s^3}{2} & qT_s^2 \end{bmatrix}. \tag{39}$$

Algorithm 2 TL-PF Primary Tracking Algorithm

Input: $\mathbf{z}_k, \hat{\boldsymbol{\eta}}_k^\star, \mathbf{P}_{\boldsymbol{\eta\eta},k}^\star, \mathbf{x}_{k-1}^{(i)}, i = 1, \ldots, N_s$

Output: $\hat{\mathbf{x}}_k, \mathbf{x}_k^{(i)}, i = 1, \ldots, N_s$

1: **for** particles, $i \leftarrow 1$ to N_s **do**
2:     Draw state particle $\mathbf{x}_k^{(i)}$ ▷ (30)
3:     Calculate TL likelihood $p(\boldsymbol{\eta}_k^\star \mid \mathbf{x}_k^{(i)})$ ▷ (31)
4:     Obtain TL weight $w_k^{\boldsymbol{\eta}(i)}$ ▷ (29)
5:     Compute measurement likelihood $p(\mathbf{z}_k \mid \mathbf{x}_k^{(i)})$ ▷ (33)
6:     Obtain weight $w_k^{(i)}$ ▷ (28)
7: **end for**

8: Normalize weights $\tilde{w}_k^{(i)} = \frac{w_k^{(i)}}{\sum_{i=1}^{N_s} w_k^{(i)}}$

9: $\left\{ \mathbf{x}_k^{\star(i)}, w_k^{\star(i)} \right\} = \text{Resample} \left\{ \mathbf{x}_k^{\star(i)}, \tilde{w}_k^{\star(i)} \right\}, i = 1, \ldots, N_s$

10: Estimate overall state posterior
     $p(\mathbf{x}_k \mid \mathbf{z}_{1:k}, \boldsymbol{\eta}_{2:k}^\star)$ ▷ (36), (37)

The initialization of the object's state and covariance in Scenario 1 are

$$\mathbf{x}_0 = [100 \text{ m}, 10 \text{ m/s}, 100 \text{ m}, 10 \text{ m/s}]^T, \tag{40}$$

$$\mathbf{P}_0 = \text{diag}[50 \text{ m}^2, 1 \text{ m}^2/\text{s}^2, 50 \text{ m}^2, 1 \text{ m}^2/\text{s}^2]. \tag{41}$$

The source and primary tracking filters observe the measurements that follow the measurement models in (3) and (4) with asymmetric measurement noise intensities. The measurement vector for each sensor comprises the object's range, $r_k = \sqrt{x_k^2 + y_k^2}$, and bearing angle, $\zeta_k = \arctan(y_k/x_k)$, i.e., $\mathbf{z}_k = [r_k, \zeta_k]^T$. The measurement noises of the source and primary tracking filters are zero-mean Gaussian denoted as $\mathbf{w}_k^\star \overset{\text{iid}}{\sim} \mathcal{N}(\mathbf{0}, \mathbf{Q}_{\mathbf{w}}^\star)$ and $\mathbf{w}_k \overset{\text{iid}}{\sim} \mathcal{N}(\mathbf{0}, \mathbf{Q}_{\mathbf{w}})$, with associated covariances $\mathbf{Q}_{\mathbf{w}}^\star = I_{\mathbf{w}}^\star \mathbf{B}_{\mathbf{w}}$ and $\mathbf{Q}_{\mathbf{w}} = I_{\mathbf{w}} \mathbf{B}_{\mathbf{w}}$, respectively, where $\mathbf{B}_{\mathbf{w}} = \text{diag}[\sigma_r^2, \sigma_\zeta^2]$. Noise intensity levels $I_{\mathbf{w}}^\star$ and $I_{\mathbf{w}}$ represent conditions impacting the individual sensors. The simulation parameters in Scenario 1 are set as $n_{\mathbf{x}} = 4$, $n_{\mathbf{z}} = 2$, $T_s = 1$ s, $q = 0.1 \text{ m}^2/\text{s}^4$, $\sigma_r = 10$ m, $\sigma_\zeta = \sqrt{10} \times 10^{-3}$ rad, $I_{\mathbf{w}}^\star = 1$, and $I_{\mathbf{w}} = 4$. The trajectory of the moving object that follows the linear motion model in (38) for 100 time steps, as shown in Fig.2.

5.1.2   Performance Evaluation

We evaluate the proposed method for Scenario 1 that provided in Fig.2 via the root-mean square error (RMSE) of the object's position for the primary tracking filter. The RMSE metric is computed by averaging $10,000$ Monte Carlo (MC) simulation iterations at time step k as:

$$\text{RMSE}(k) = \sqrt{\frac{1}{MC} \sum_{m=1}^{MC} (\text{True Pos.}_{m,k} - \text{Est. Pos.}_{m,k})^2}. \tag{42}$$

Figure 3 shows RMSE results for TL-PF ($N_s = 6000$ particles) compared with TL-UKF and third-degree TL-CKF. As shown in Fig. 3, the proposed TL-PF algorithm (blue dashed line with + marks) has lower RMSE values at the entire duration of the tracked trajectory compared to the isolated PF (blue solid line with + marks). For instance, the TL-PF is able to achieve RMSE value of 4.28 m at time step $k = 52$ s, while the isolated PF has RMSE value of 7.37 m at the same time step. Compared with previously proposed algorithms, the TL-UKF (green dashed line with △ marks) and third-degree TL-CKF (red dashed line with □ marks) achieve RMSE values of 10.13 m and 11.28 m, respectively, at the same time step $k = 52$ s. For the entire duration of the object trajectory in Scenario 1, the TL-PF algorithm performs better with lower RMSE values compared to comparable algorithms with BTLF and isolated (without incorporation of the transfer learning approach).
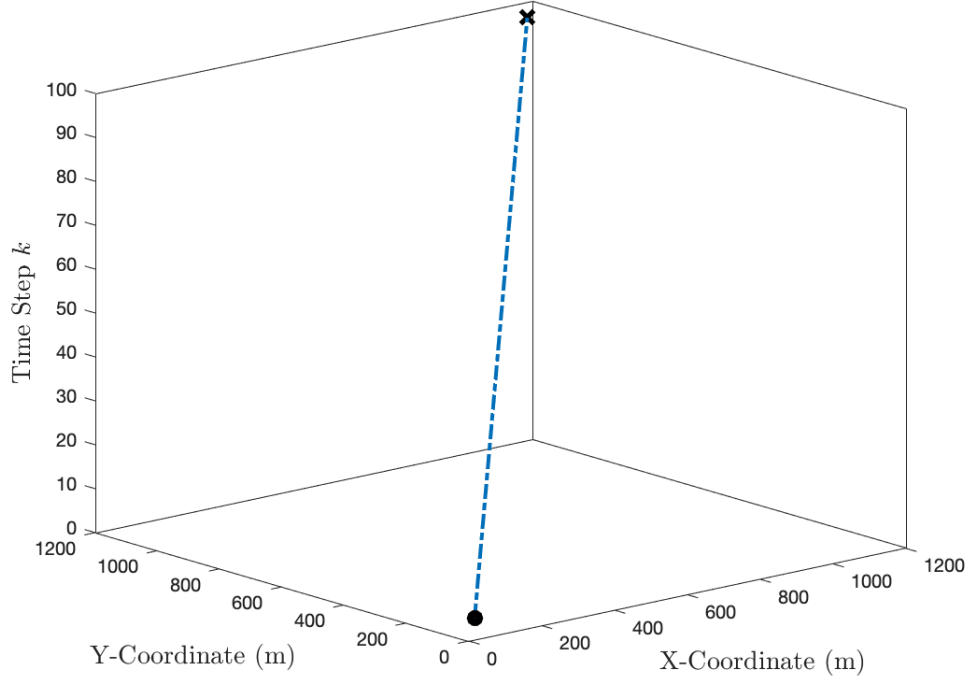
Figure 2: Scenario 1: A moving object trajectory in two-dimensional coordinates with an initial point indicated by ●.
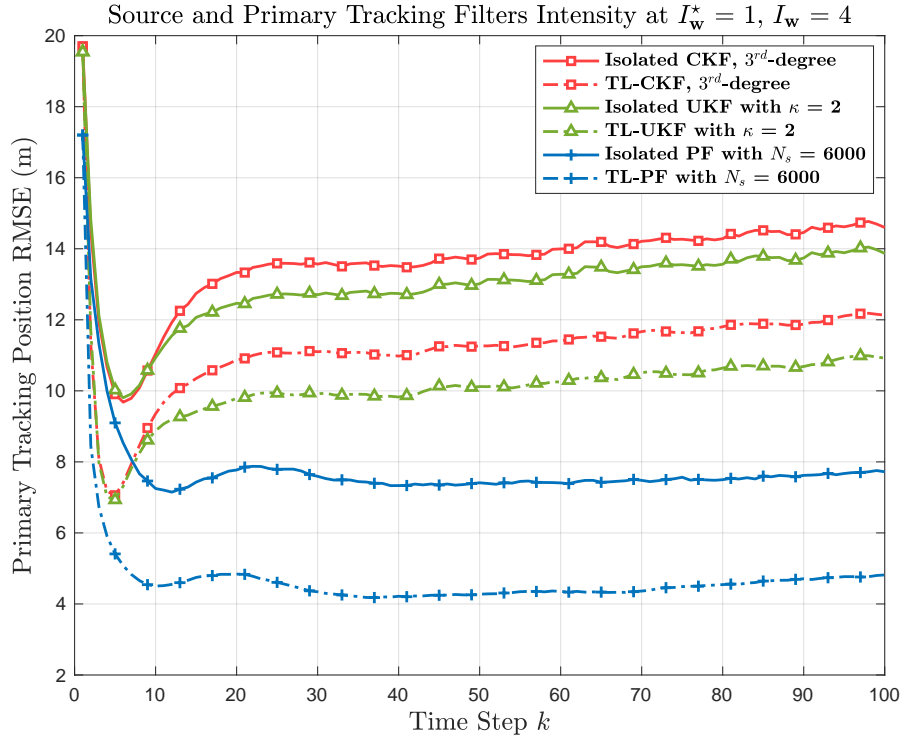

Figure 3: Scenario 1: RMSE values plots computed via (42) for the proposed TL-PF (blue line with + marks) algorithm along with isolated and BTLF of UKF (green line with △ marks) and third-degree CKF (red line with □ marks).

5.2 Scenario 2: Nonlinear Maneuvering Motion Model

5.2.1 Tracking System Model

For our simulations, we consider a single maneuvering object with an unknown state vector to be tracked by a dual-tracking system. We adopt the nonlinear motion model in [37] given by

$$
\mathbf{x}_k = \begin{bmatrix}
1 & \frac{\sin(\Omega_{k-1}T_s)}{\Omega_{k-1}} & 0 & -\left(\frac{1-\cos(\Omega_{k-1}T_s)}{\Omega_{k-1}}\right) & 0 \\
0 & \cos(\Omega_{k-1}T_s) & 0 & -\sin(\Omega_{k-1}T_s) & 0 \\
0 & \frac{1-\cos(\Omega_{k-1}T_s)}{\Omega_{k-1}} & 1 & \frac{\sin(\Omega_{k-1}T_s)}{\Omega_{k-1}} & 0 \\
0 & \sin(\Omega_{k-1}T_s) & 0 & \cos(\Omega_{k-1}T_s) & 0 \\
0 & 0 & 0 & 0 & 1
\end{bmatrix} \mathbf{x}_{k-1}
$$
$$
+ \mathbf{v}_{k-1}. \tag{43}
$$

The object state is given by $\mathbf{x}_k = [x_k, \dot{x}_k, y_k, \dot{y}_k, \Omega_k]^T$, which consists of the Cartesian coordinates of the object's position (x_k, y_k), the object's velocity $(\dot{x}_k, \dot{y}_k)$, and the turn rate Ω_k. The process noise $\mathbf{v}_{k-1} \overset{\text{iid}}{\sim} \mathcal{N}(0, \mathbf{Q_v})$ with associated covariance

$$
\mathbf{Q_v} = \begin{bmatrix}
q_1\frac{T_s^4}{4} & q_1\frac{T_s^3}{2} & 0 & 0 & 0 \\
q_1\frac{T_s^3}{2} & q_1 T_s^2 & 0 & 0 & 0 \\
0 & 0 & q_1\frac{T_s^4}{4} & q_1\frac{T_s^3}{2} & 0 \\
0 & 0 & q_1\frac{T_s^3}{2} & q_1 T_s^2 & 0 \\
0 & 0 & 0 & 0 & q_2 T_s
\end{bmatrix}. \tag{44}
$$

As in Section 2.2, the error process noise covariances of the source and primary tracking filters are assumed to be identical.

5.2.2 Parameters Settings

The simulation parameter settings for the dual-tracking system are specified in Table 1. The object maneuvers in a two-dimensional trajectory with a duration of 100 time steps as shown in Fig.4. The object's state and covariance are initialized as:

$$
\mathbf{x}_0 = [1000 \text{ m}, 300 \text{ m/s}, 1000 \text{ m}, 0 \text{ m/s}, -3°/\text{s}]^T, \tag{45}
$$
$$
\mathbf{P}_0 = \text{diag}[100 \text{ m}^2, 10 \text{ m}^2/\text{s}^2, 100 \text{ m}^2, 10 \text{ m}^2/\text{s}^2,
$$
$$
100 \times 10^{-3} \text{ rad}^2/\text{s}^2]. \tag{46}
$$

The performance results are evaluated by averaging $10,000$ MC simulation runs. The object trajectory and parameter settings are identical to the simulation realization in [21, 30] to present a fair comparison with the previous results obtained from incorporating BTLF into the UKF and CKF local approximation approaches.

5.2.3 Performance Evaluation

Similarly, we evaluate the proposed TL-PF using the tracking Scenario 2 in Fig.4. The performance metric of interest is the RMSE of the object's position (x_k, y_k) for the primary tracking filter. The performance of the proposed TL-PF and isolated PF are evaluated in terms of RMSE per time step provided in Fig. 5 in addition to isolated and incorporating transfer learning of local approaches, UKF and third-degree CKF, previously presented in [30]. The proposed TL-PF algorithm with $N_s = 6000$ particles (blue dashed line with + marks) achieves RMSE values of 7.85 m and 14.38 m at time steps $k = 48$ s and $k = 75$ s, respectively, under the noise intensities of $I_\mathbf{w} = 4$ (primary sensor) and $I_\mathbf{w}^\star = 1$ (source sensor). In comparison, the isolated version of PF (blue solid line) has RMSE values of 9.73 m and 17.34 m at the same noise level and time steps. Furthermore, the proposed TL-PF algorithm (with $N_s = 6000$) achieves an RMSE of 13.10 m at time step $k = 10$ s, outperforming the third-degree TL-CKF and TL-UKF (with $\kappa = 2$), which obtain RMSE values of 15.72 m and 14.35 m, respectively, under the same conditions. From Fig. 5, we see that the performance of the proposed TL-PF is always superior to that of isolated approaches. For most of the trajectory, TL-PF performs significantly better than TL-CKF and TL-UKF. In the intervals of $(20, 40)$ s and $(85, 95)$ s, TL-PF performs comparably to TL-CKF and TL-UKF. However, we note that the performance of TL-PF can be further improved by increasing the number of particles, N_s, at the expense of higher computational cost.

Furthermore, the RMSE curves of the algorithms presented in Fig. 5 have fluctuations in the interval of $(40, 75)$ s. We compare the performance results from Scenario 1 (Fig. 3) with those from Scenario 2 (Fig.5). We note that the

Table 1: Scenario 2: Simulation Parameter Settings

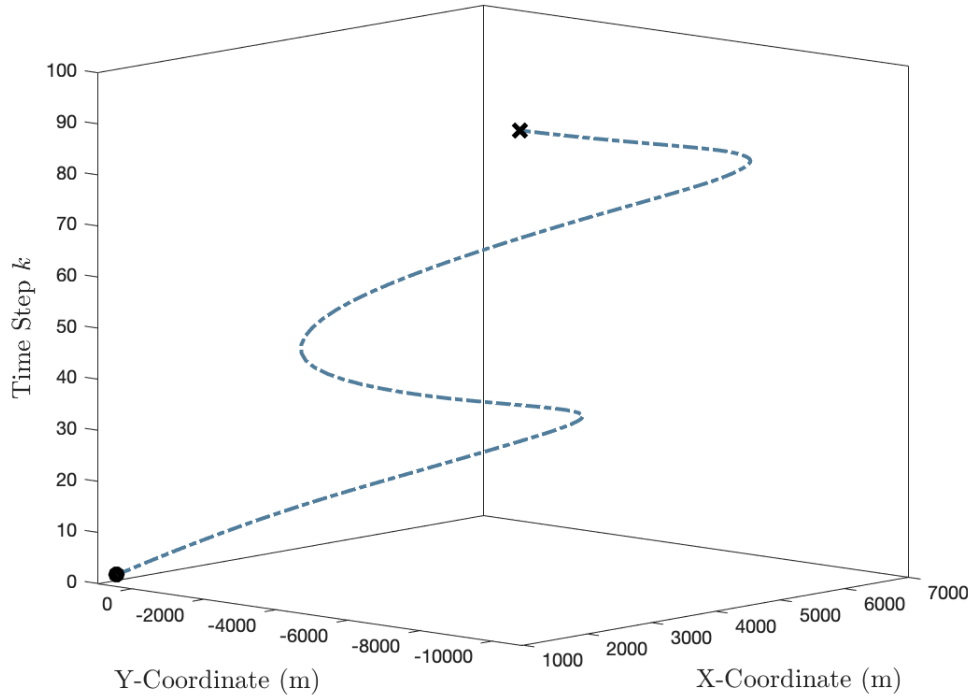| Parameter	Value	Parameter	Value
$n_\mathbf{x}$	5	$n_\mathbf{z}$	2
T_s	1 s	K	100
MC runs	10,000	κ	2
q_1	$0.1\ \mathrm{m^2/s^4}$	q_2	$1.75 \times 10^{-2}\ \mathrm{rad^2/s^3}$
σ_r	10 m	σ_ζ	$\sqrt{10} \times 10^{-3}\ \mathrm{rad}$
$I_\mathbf{w}^\star$	1	$I_\mathbf{w}$	$1 \rightarrow 8$

Figure 4: Scenario 2: A trajectory of an object maneuvering in two-dimensional Cartesian space with time shown vertically, where ● and ✖ indicate the initial and end points, respectively.
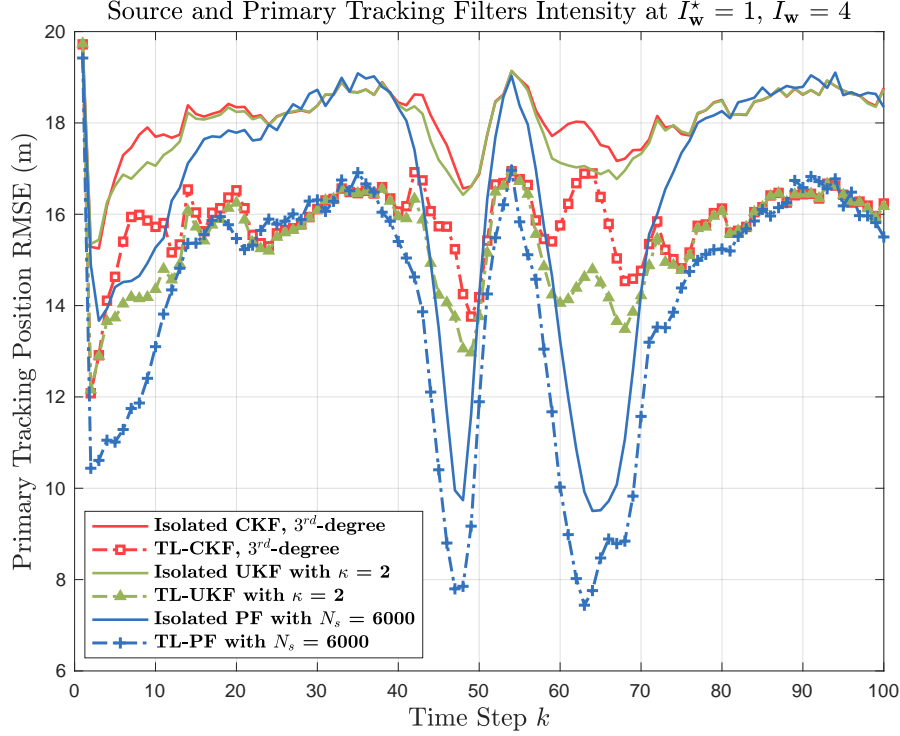
Figure 5: Scenario 2: A comparison of obtained RMSE performance plots versus time step for the proposed algorithm TL-PF (blue dashed line with + marks), TL-UKF [30], TL-CKF [30], and isolated filters.

fluctuations in the interval of $(40, 75)$ s are due to the nature of the maneuvering trajectory where the object track has high maneuvering turns in the same time interval, as obviously shown in Fig. 4. During this time interval, the proposed TL-PF demonstrates significant strength in capturing object maneuvering turns and estimates the object's position more accurately with lower RMSE values compared to other plotted algorithms. For example, the TL-PF algorithm (with $N_s = 6000$) achieves an RMSE value of 7.79 m during the high maneuvering turns interval at time step $k = 47$ s, while the TL-UKF (green dashed line) has an RMSE value of 13.75 m.

5.2.4   Overall Performance Gain

To further demonstrate the behavior of the proposed TL-PF algorithm, we evaluate its overall RMSE performance, averaged over 100 time steps and $10{,}000$ MC iterations, under various levels of primary noise intensity $I_{\mathbf{w}}$, while fixing the intensity level of source noise $I_{\mathbf{w}}^\star$ as follows:

$$\text{Overall RMSE} = \frac{1}{K} \sum_{k=1}^{K} \sqrt{\frac{1}{MC} \sum_{m=1}^{MC} (\text{True Pos.}_{m,k} - \text{Est. Pos.}_{m,k})^2}. \qquad (47)$$

As shown in Fig. 6, the accuracy gain of the TL-PF (blue dashed line marked with $*$) compared to the isolated traditional PF increases as the level of primary noise intensity $I_{\mathbf{w}}$ increases. For instance, under $I_{\mathbf{w}} = 4$, the TL-PF (with $N_s = 6000$) achieves an RMSE value of 14.33 m, while the isolated PF has an RMSE of 16.74 m with a reduction in estimation error of approximately 2.41 m. Similarly, under $I_{\mathbf{w}} = 8$, the TL-PF has an RMSE of 17.45 m compared to 23.06 m for the isolated PF with a reduction of 5.61 m. Furthermore, the TL-PF (with $N_s = 6000$) outperforms the fifth-degree TL-CKF (green dashed line with $\triangledown$ marks) and is capable of achieving an accuracy gain value of approximately 1.24 m under a level of primary noise intensity $I_{\mathbf{w}} = 8$.

To investigate the performance gain of incorporating BTLF into several tracking algorithms, we evaluate the primary tracking position RMSE gain of using BTLF compared to isolated filters calculated as

$$\Delta \text{RMSE} = \text{RMSE}^{\text{Isolated}} - \text{RMSE}^{\text{TL}}, \qquad (48)$$
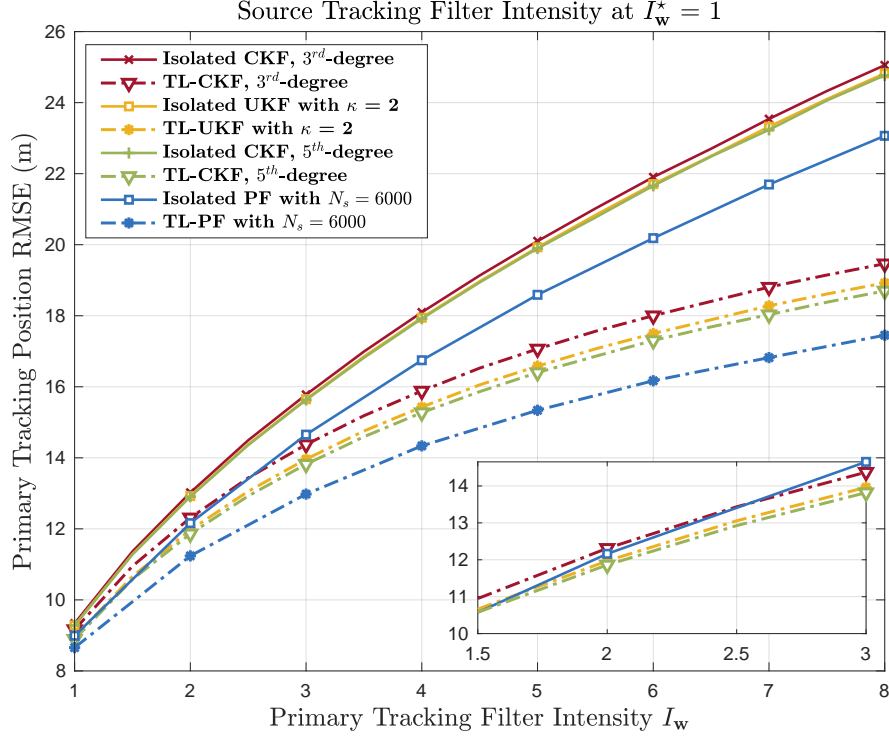
13

Figure 6: Scenario 2: The overall RMSE performance of the proposed TL-PF algorithm (with $N_s = 6000$) under varying primary noise intensity $I_{\mathbf{w}}$, plotted alongside the performance of local BTLF approaches in [30].

under varying $\Delta I_{\mathbf{w}}$, which is the absolute value of the difference between the primary and source noise intensities computed as

$$\Delta I_{\mathbf{w}} = |I_{\mathbf{w}} - I_{\mathbf{w}}^\star|. \tag{49}$$

As shown in Fig. 7, the ΔRMSE for third-degree CKF, UKF, fifth-degree CKF, and PF (with $N_s = 6000$) increases as the absolute difference between the primary and source noise intensities $\Delta I_{\mathbf{w}}$ increases. This describes the proportional relationship between ΔRMSE and $\Delta I_{\mathbf{w}}$ where ΔRMSE increases almost linearly. For instance, at $\Delta I_{\mathbf{w}} = 3$, the PF (with $N_s = 6000$) and third-degree CKF achieve ΔRMSE values of 2.41 m and 2.21 m, respectively. However, the PF (with $N_s = 6000$) has ΔRMSE value of approximately 5.61 m, which is less than ΔRMSE value of 6.06 m for the fifth-degree CKF at $\Delta I_{\mathbf{w}} = 7$. We note that the fifth-degree CKF performs significantly better in terms of the primary tracking position RMSE gain ΔRMSE for most of the absolute difference values between the primary and source noise intensities $\Delta I_{\mathbf{w}}$, as illustrated in Fig. 7. These ΔRMSE curves can serve as a guideline for whether BTLF can be incorporated in a certain system depending on the difference between the intensities of the noise.

5.2.5   Varying Particles Number and Computational Time

To investigate the effect of particles number on the accuracy performance of the proposed TL-PF algorithm, we performed a simulation analysis with varying number of particles $N_s = 3000 \rightarrow 12000$ under noise intensity levels at $I_{\mathbf{w}}^\star = 1$ and $I_{\mathbf{w}} = 4$. The obtained results, shown in Fig. 8, represent that increasing the number of particles N_s leads to higher accuracy performance (lower value of RMSE) for both the TL-PF and isolated PF algorithms. This describes the inverse proportional relationship between the RMSE and the number of particles. Furthermore, the computational time per time step k, evaluated on a laptop with a 3.1 GHz Core i7 processor, of both the TL-PF (bottom plot with green dashed line) and isolated PF (top plot with green solid line) is proportional to the number utilized. Moreover, the sensitivity level of the proposed TL-PF algorithm to the number of particles is greater than the isolated version of PF. For instance, with $N_s = 3000$ particles, the TL-PF achieves RMSE of 15.23 m, while the isolated PF has an RMSE of 16.95 m. By increasing the number of particles to $N_s = 12000$, the RMSE of TL-PF improves to 14.07 m, while the RMSE of isolated PF improves only to 16.66 m. As the number of particles increases from 3000 to 12000, the TL-PF gains an accuracy of 1.16 m compared to 0.29 m for the isolated PF. Table 2 presents a comparative analysis of local and global approaches integrated with BTLF and their corresponding isolated filters in terms of RMSE and
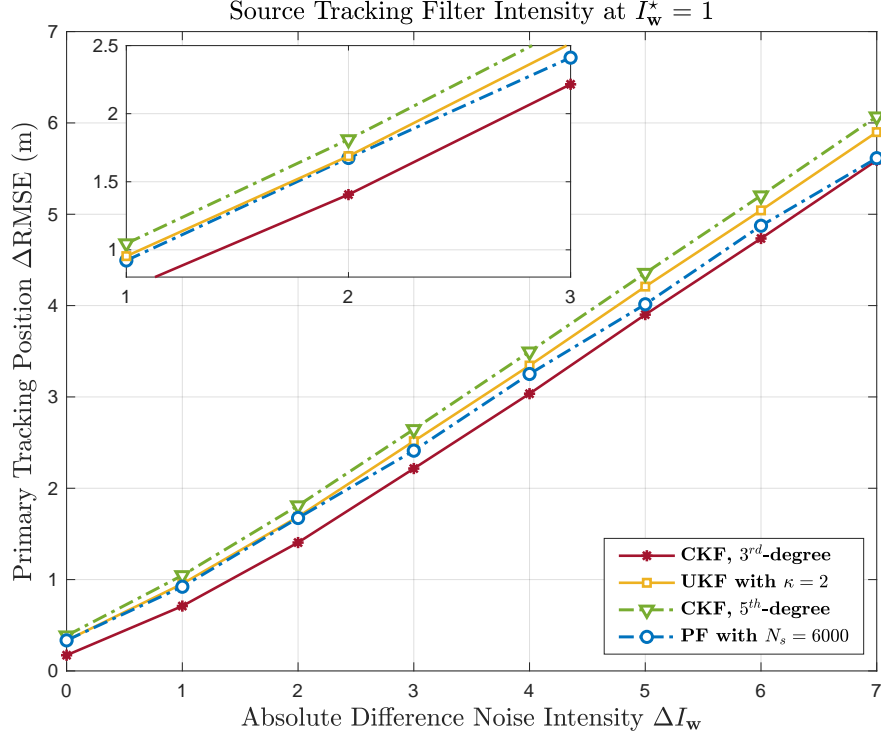
Figure 7: Scenario 2: The RMSE gain ΔRMSE of incorporating BTL for third-degree CKF (maroon solid line), UKF (yellow solid line), fifth-degree CKF (green dashed line), and PF (blue dashed line) versus the absolute difference between the primary and source noise intensities $\Delta I_{\mathbf{w}}$.

computational process time per time step. Note that the RMSE results for the first three rows in Table 2, which represent local approaches, have previously been obtained in [30]. These results are included in this article to provide a comparative baseline for the proposed algorithm using the global approach. Table 2 shows that integrating of the global approach, PF, with BTLF achieves a superior reduction in RMSE results compared to RMSE performances of TL-UKF, third-degree TL-CKF, and fifth-degree TL-CKF. This RMSE improvement comes with a modest increase in processing time, from 0.296 ms (fifth-degree TL-CKF) to 0.931 ms (TL-PF with $N_s = 3000$), as shown in Table 2.

6   Conclusion

We developed a BTL approach for particle filtering, TL-PF, in a dual-tracking system with asymmetric measurement noise intensities at the primary and source sensors. By leveraging predicted measurement information transferred from the source sensor, the primary sensor, which experiences the higher noise intensity, is able to achieve a significant gain in tracking performance compared to an isolated particle filter, without applying transfer learning. We also compared the performance of the proposed transfer learning particle filter schemes with earlier schemes based on applying Bayesian transfer learning to the unscented Kalman filter and the cubature Kalman filter, referred to as TL-UKF and TL-CKF, respectively. Furthermore, the TL-PF shows greater sensitivity to the number of particles compared to the isolated particle filter. Although increasing the number of particles improves tracking performance, it also increases computational time, which can be a challenge in real-time processing scenarios. However, a moderate number of particles can be effectively utilized in certain applications, particularly with the advancements in hardware technology that allow for greater computational efficiency. For the number of particles $N_s = 6000$, the process times per step are approximately 2 ms and 1.9 ms for the TL-PF and the isolated particle filter, respectively. Furthermore, we observe from the numerical results that the relative gain of the TL-PF is linearly proportional to the absolute difference value between the source and primary sensors.

For future work, it would be interesting to explore a hybrid system that incorporates a decision step at either the source or the primary sensor to determine whether to perform transfer learning at each time step. In addition, the framework can be generalized to involve more than a single source tracking system by transferring predicted observa-
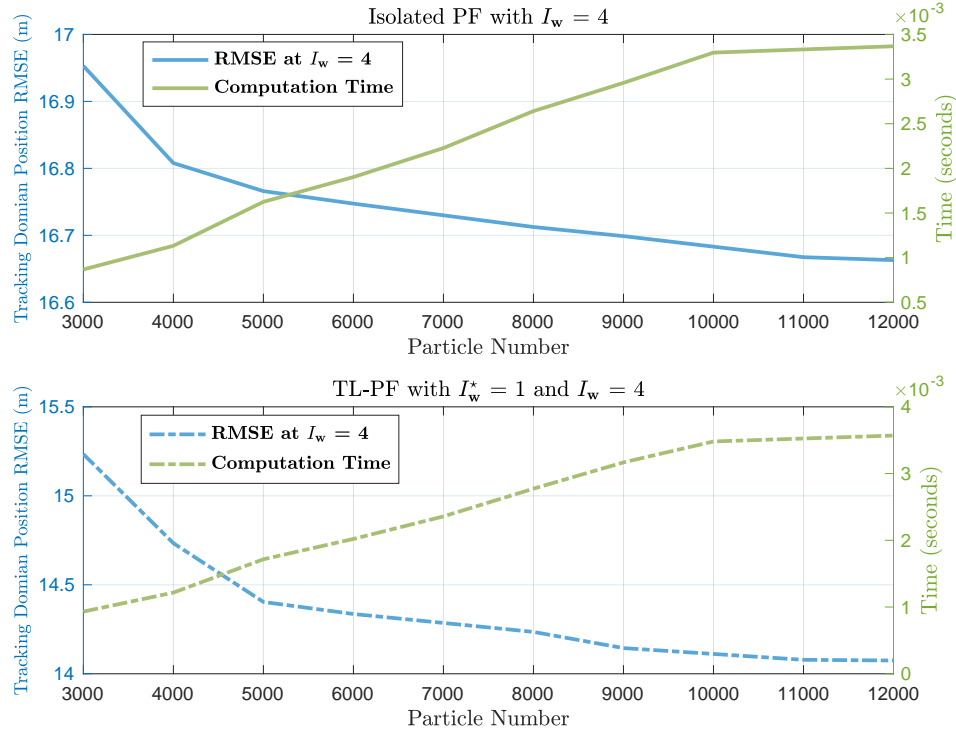
Figure 8: Scenario 2: RMSE (blue) and the computation time (green) curves of isolated (top) and incorporating transfer learning (bottom) for PF at primary noise intensity $I_{\mathbf{w}} = 4$.

Table 2: Scenario 2: Position RMSE and Computation Time for Primary Tracking Filters with $I_{\mathbf{w}} = 4$

Filter	Points	Isolated		BTLF	
		RMSE (m)	Time per Step (ms)	RMSE (m)	Time per Step (ms)
CKF, 3rd-degree	10	18.0973	0.154	15.8815	0.188
UKF, $\kappa = 2$	11	17.9451	0.165	15.4299	0.206
CKF, 5th-degree	51	17.9178	0.225	15.2728	0.297
SIR-PF	3000	16.9530	0.867	15.2341	0.931
SIR-PF	6000	16.7473	1.902	14.3359	2.020
SIR-PF	9000	16.6988	2.957	14.1443	3.167
SIR-PF	12000	16.6630	3.367	14.0746	3.569

tions and feeding them into the primary tracking system using the proposed TL-PF. Moreover, investigating hardware acceleration approaches to reduce the computational time of TL-PF is another promising direction for future work.

A   Particle Filter with Bayesian Transfer Learning Derivation

A.1   Source Tracking Filter

The object state posterior density in (10) is given by

$$p(\mathbf{x}_{0:k}^{\star} \mid \mathbf{z}_{1:k}^{\star}) \approx \sum_{i=1}^{N_s} w_k^{\star(i)} \delta\left(\mathbf{x}_{0:k}^{\star} - \mathbf{x}_{0:k}^{\star(i)}\right), \tag{50}$$

and associated particle weights are computed as

$$w_k^{\star(i)} \propto \frac{p(\mathbf{x}_{0:k}^{\star(i)} \mid \mathbf{z}_{1:k}^{\star})}{q(\mathbf{x}_{0:k}^{\star(i)} \mid \mathbf{z}_{1:k}^{\star})}. \tag{51}$$

The numerator in (51) can be written as

$$
\begin{aligned}
p(\mathbf{x}_{0:k}^{\star(i)} \mid \mathbf{z}_{1:k}^{\star}) &= p(\mathbf{x}_{0:k}^{\star(i)} \mid \mathbf{z}_k^{\star}, \mathbf{z}_{1:k-1}^{\star}) \\
&= \frac{p(\mathbf{z}_k^{\star} \mid \mathbf{x}_{0:k}^{\star(i)}, \mathbf{z}_{1:k-1}^{\star})\, p(\mathbf{x}_{0:k}^{\star(i)} \mid \mathbf{z}_{1:k-1}^{\star})}{p(\mathbf{z}_k^{\star} \mid \mathbf{z}_{1:k-1}^{\star})},
\end{aligned} \tag{52}
$$

where $p(\mathbf{z}_k^{\star} \mid \mathbf{x}_{0:k}^{\star(i)}, \mathbf{z}_{1:k-1}^{\star}) = p(\mathbf{z}_k^{\star} \mid \mathbf{x}_k^{\star(i)})$ is due to the fact that the measurement $\mathbf{z}_k^{\star}$ given the current state $\mathbf{x}_k^{\star(i)}$ is conditionally independent of all previous states $\mathbf{x}_{0:k-1}^{\star(i)}$ and measurements $\mathbf{z}_{1:k-1}^{\star}$, and $p(\mathbf{x}_{0:k}^{\star(i)} \mid \mathbf{z}_{1:k-1}^{\star}) = p(\mathbf{x}_k^{\star(i)} \mid \mathbf{x}_{k-1}^{\star(i)})\, p(\mathbf{x}_{0:k-1}^{\star(i)} \mid \mathbf{z}_{1:k-1}^{\star})$ is derived according to the first-order Markov chain assumption. Furthermore, the density $p(\mathbf{x}_{0:k}^{\star(i)} \mid \mathbf{z}_{1:k}^{\star})$ in (52) can be rewritten as

$$p(\mathbf{x}_{0:k}^{\star(i)} \mid \mathbf{z}_{1:k}^{\star}) \propto p(\mathbf{z}_k^{\star} \mid \mathbf{x}_k^{\star(i)})\, p(\mathbf{x}_k^{\star(i)} \mid \mathbf{x}_{k-1}^{\star(i)})\, p(\mathbf{x}_{0:k-1}^{\star(i)} \mid \mathbf{z}_{1:k-1}^{\star}). \tag{53}$$

The denominator in (51) can be factorized similarly to [34] as

$$q(\mathbf{x}_{0:k}^{\star(i)} \mid \mathbf{z}_{1:k}^{\star}) = q(\mathbf{x}_k^{\star(i)} \mid \mathbf{x}_{0:k-1}^{\star(i)}, \mathbf{z}_{1:k}^{\star})\, q(\mathbf{x}_{0:k-1}^{\star(i)} \mid \mathbf{z}_{1:k-1}^{\star}), \tag{54}$$

where $q(\mathbf{x}_k^{\star(i)} \mid \mathbf{x}_{0:k-1}^{\star(i)}, \mathbf{z}_{1:k}^{\star}) = q(\mathbf{x}_k^{\star(i)} \mid \mathbf{x}_{k-1}^{\star(i)}, \mathbf{z}_{1:k}^{\star})$ due to the dependency only on $\mathbf{x}_{k-1}^{\star(i)}$ and conditionally independent of all previous states $\mathbf{x}_{0:k-2}^{\star(i)}$. Therefore, the particle weights can be rewritten by substituting (53) and (54) into (51) as

$$w_k^{\star(i)} \propto w_{k-1}^{\star(i)} \frac{p(\mathbf{z}_k^{\star} \mid \mathbf{x}_k^{\star(i)})\, p(\mathbf{x}_k^{\star(i)} \mid \mathbf{x}_{k-1}^{\star(i)})}{q(\mathbf{x}_k^{\star(i)} \mid \mathbf{x}_{k-1}^{\star(i)}, \mathbf{z}_{1:k}^{\star})}. \tag{55}$$

The predicted observation posterior density in (19) is approximated by weighted particles as

$$p(\boldsymbol{\eta}_{1:k+1}^{\star} \mid \mathbf{z}_{1:k}^{\star}) \approx \sum_{i=1}^{N_s} w_{k+1}^{\star\boldsymbol{\eta}(i)} \delta\left(\boldsymbol{\eta}_{1:k+1}^{\star} - \boldsymbol{\eta}_{1:k+1}^{\star(i)}\right). \tag{56}$$

The weights $w_{k+1}^{\star\boldsymbol{\eta}(i)}$ in (56) are computed as

$$w_{k+1}^{\star\boldsymbol{\eta}(i)} \propto \frac{p(\boldsymbol{\eta}_{1:k+1}^{\star(i)} \mid \mathbf{z}_{1:k}^{\star})}{q(\boldsymbol{\eta}_{1:k+1}^{\star(i)} \mid \mathbf{z}_{1:k}^{\star})}, \tag{57}$$

where the numerator $p(\boldsymbol{\eta}_{1:k+1}^{\star(i)} \mid \mathbf{z}_{1:k}^{\star})$ can be written as

$$
\begin{aligned}
p(\boldsymbol{\eta}_{1:k+1}^{\star(i)} \mid \mathbf{z}_{1:k}^{\star}) &= p(\boldsymbol{\eta}_{k+1}^{\star(i)}, \boldsymbol{\eta}_{1:k}^{\star(i)} \mid \mathbf{z}_{1:k}^{\star}) \\
&= p(\boldsymbol{\eta}_{k+1}^{\star(i)} \mid \mathbf{x}_{0:k+1}^{\star(i)}, \mathbf{z}_{1:k}^{\star}, \boldsymbol{\eta}_{1:k}^{\star(i)})\, p(\mathbf{x}_{0:k+1}^{\star(i)} \mid \mathbf{z}_{1:k}^{\star}, \boldsymbol{\eta}_{1:k}^{\star(i)}).
\end{aligned} \tag{58}
$$

Similarly to deriving particle weights of the object state density, the predicted observation $\boldsymbol{\eta}_{k+1}^{\star(i)}$ depends only on the predicted state $\mathbf{x}_{k+1}^{\star(i)}$ and is conditionally independent of all previous states $\mathbf{x}_{0:k}^{\star(i)}$ and measurements $\mathbf{z}_{1:k}^{\star}$ resulting in $p(\boldsymbol{\eta}_{k+1}^{\star(i)} \mid \mathbf{x}_{0:k+1}^{\star(i)}, \mathbf{z}_{1:k}^{\star}, \boldsymbol{\eta}_{1:k}^{\star(i)}) = p(\boldsymbol{\eta}_{k+1}^{\star(i)} \mid \mathbf{x}_{k+1}^{\star(i)})$. Furthermore, the second term $p(\mathbf{x}_{0:k+1}^{\star(i)} \mid \mathbf{z}_{1:k}^{\star}, \boldsymbol{\eta}_{1:k}^{\star(i)})$ in (58) can be written as

$$p(\mathbf{x}_{0:k+1}^{\star(i)} \mid \mathbf{z}_{1:k}^{\star}, \boldsymbol{\eta}_{1:k}^{\star(i)}) = p(\mathbf{x}_{k+1}^{\star(i)} \mid \mathbf{x}_{0:k}^{\star(i)}, \mathbf{z}_{1:k}^{\star}, \boldsymbol{\eta}_{1:k}^{\star(i)}) \, p(\mathbf{x}_{0:k}^{\star(i)} \mid \mathbf{z}_{1:k}^{\star}, \boldsymbol{\eta}_{1:k}^{\star(i)}) \tag{59}$$

$$= p(\mathbf{x}_{k+1}^{\star(i)} \mid \mathbf{x}_{k}^{\star(i)}) \, p(\mathbf{x}_{0:k}^{\star(i)} \mid \mathbf{z}_{1:k}^{\star}), \tag{60}$$

where simplification from (59) to (60) due to the first-order Markov chain assumption and to conditionally independent of self-predicted observations $\boldsymbol{\eta}_{1:k}^{\star(i)}$. The denominator in (57) can be factorized as

$$q(\boldsymbol{\eta}_{1:k+1}^{\star(i)} \mid \mathbf{z}_{1:k}^{\star}) = q(\boldsymbol{\eta}_{k+1}^{\star(i)} \mid \mathbf{x}_{0:k}^{\star(i)}, \mathbf{z}_{1:k}^{\star}, \boldsymbol{\eta}_{1:k}^{\star(i)}) \, q(\mathbf{x}_{0:k}^{\star(i)} \mid \mathbf{z}_{1:k}^{\star}, \boldsymbol{\eta}_{1:k}^{\star(i)}), \tag{61}$$

where $q(\mathbf{x}_{0:k}^{\star(i)} \mid \mathbf{z}_{1:k}^{\star}, \boldsymbol{\eta}_{1:k}^{\star(i)}) = q(\mathbf{x}_{0:k}^{\star(i)} \mid \mathbf{z}_{1:k}^{\star})$ is due to the conditionally independent of the self-predicted observations. Moreover, the predicted observation $\boldsymbol{\eta}_{k+1}^{\star(i)}$ given the current state $\mathbf{x}_{k}^{\star(i)}$ is conditionally independent of all previous states $\mathbf{x}_{0:k-1}^{\star(i)}$ and predicted observations $\boldsymbol{\eta}_{1:k}^{\star(i)}$ yielding to

$$q(\boldsymbol{\eta}_{k+1}^{\star(i)} \mid \mathbf{x}_{0:k}^{\star(i)}, \mathbf{z}_{1:k}^{\star}, \boldsymbol{\eta}_{1:k}^{\star(i)}) = q(\boldsymbol{\eta}_{k+1}^{\star(i)} \mid \mathbf{x}_{k}^{\star(i)}, \mathbf{z}_{1:k}^{\star}). \tag{62}$$

By substituting derived and simplified densities from (58) to (62) into (57), the weights $w_{k+1}^{\star\boldsymbol{\eta}(i)}$ can be rewritten as

$$w_{k+1}^{\star\boldsymbol{\eta}(i)} \propto w_{k}^{\star(i)} \, \frac{p(\boldsymbol{\eta}_{k+1}^{\star(i)} \mid \mathbf{x}_{k+1}^{\star(i)}) \, p(\mathbf{x}_{k+1}^{\star(i)} \mid \mathbf{x}_{k}^{\star(i)})}{q(\boldsymbol{\eta}_{k+1}^{\star(i)} \mid \mathbf{x}_{k}^{\star(i)}, \mathbf{z}_{1:k}^{\star})}. \tag{63}$$

A.2   Primary Tracking Filter

The overall posterior density that leverages transferred knowledge from the source tracking filter in (26) is approximately computed via weighted particles as

$$p(\mathbf{x}_k \mid \mathbf{z}_{1:k}, \boldsymbol{\eta}_{2:k}^{\star}) \approx \sum_{i=1}^{N_s} w_k^{(i)} \delta\left(\mathbf{x}_k - \mathbf{x}_k^{(i)}\right), \tag{64}$$

and associated weights $w_k^{(i)}$ are defined as

$$w_k^{(i)} \propto \frac{p(\mathbf{x}_{0:k}^{(i)} \mid \mathbf{z}_{1:k}, \boldsymbol{\eta}_{2:k}^{\star})}{q(\mathbf{x}_{0:k}^{(i)} \mid \mathbf{z}_{1:k}, \boldsymbol{\eta}_{2:k}^{\star})}. \tag{65}$$

The numerator in (65) can be factorized for derivation as $p(\mathbf{x}_{0:k}^{(i)} \mid \mathbf{z}_{1:k}, \boldsymbol{\eta}_{2:k}^{\star}) = p(\mathbf{x}_{0:k}^{(i)} \mid \mathbf{z}_k, \mathbf{z}_{1:k-1}, \boldsymbol{\eta}_k^{\star}, \boldsymbol{\eta}_{2:k-1}^{\star})$ and written as

$$p(\mathbf{x}_{0:k}^{(i)} \mid \mathbf{z}_k, \mathbf{z}_{1:k-1}, \boldsymbol{\eta}_k^{\star}, \boldsymbol{\eta}_{2:k-1}^{\star}) =$$
$$\frac{p(\mathbf{z}_k \mid \mathbf{x}_{0:k}^{(i)}, \mathbf{z}_{1:k-1}, \boldsymbol{\eta}_k^{\star}, \boldsymbol{\eta}_{2:k-1}^{\star}) \, p(\boldsymbol{\eta}_k^{\star} \mid \mathbf{x}_{0:k}^{(i)}, \mathbf{z}_{1:k-1}, \boldsymbol{\eta}_{2:k-1}^{\star})}{p(\mathbf{z}_k \mid \mathbf{z}_{1:k-1}) \, p(\boldsymbol{\eta}_k^{\star} \mid \boldsymbol{\eta}_{2:k-1}^{\star})} \cdot p(\mathbf{x}_{0:k}^{(i)} \mid \mathbf{z}_{1:k-1}, \boldsymbol{\eta}_{2:k-1}^{\star}), \tag{66}$$

where $p(\mathbf{z}_k \mid \mathbf{x}_{0:k}^{(i)}, \mathbf{z}_{1:k-1}, \boldsymbol{\eta}_k^{\star}, \boldsymbol{\eta}_{2:k-1}^{\star}) = p(\mathbf{z}_k \mid \mathbf{x}_k^{(i)})$ and $p(\boldsymbol{\eta}_k^{\star} \mid \mathbf{x}_{0:k}^{(i)}, \mathbf{z}_{1:k-1}, \boldsymbol{\eta}_{2:k-1}^{\star}) = p(\boldsymbol{\eta}_k^{\star} \mid \mathbf{x}_k^{(i)})$ are due to the conditional independency between the measurement $\mathbf{z}_k$, the predicted observation $\boldsymbol{\eta}_k^{\star}$, all previous states $\mathbf{x}_{0:k-1}^{(i)}$, all previous measurements $\mathbf{z}_{1:k-1}$, and all previous predicted observations $\boldsymbol{\eta}_{2:k-1}^{\star}$ given the current state $\mathbf{x}_k^{(i)}$. The last term on the right-hand side (R.H.S) in (66) can be derived on the basis of the first-order Markov chain assumption as $p(\mathbf{x}_{0:k}^{(i)} \mid \mathbf{z}_{1:k-1}, \boldsymbol{\eta}_{2:k-1}^{\star}) = p(\mathbf{x}_k^{(i)} \mid \mathbf{x}_{k-1}^{(i)}) \, p(\mathbf{x}_{0:k-1}^{(i)} \mid \mathbf{z}_{1:k-1}, \boldsymbol{\eta}_{2:k-1}^{\star})$. Therefore, the density $p(\mathbf{x}_{0:k}^{(i)} \mid \mathbf{z}_{1:k}, \boldsymbol{\eta}_{2:k}^{\star})$ of the numerator in (65) is simplified and rewritten as

$$p(\mathbf{x}_{0:k}^{(i)} \mid \mathbf{z}_{1:k}, \boldsymbol{\eta}_{2:k}^{\star}) \propto p(\mathbf{z}_k \mid \mathbf{x}_k^{(i)}) \, p(\boldsymbol{\eta}_k^{\star} \mid \mathbf{x}_k^{(i)}) p(\mathbf{x}_k^{(i)} \mid \mathbf{x}_{k-1}^{(i)}) \, p(\mathbf{x}_{0:k-1}^{(i)} \mid \mathbf{z}_{1:k-1}, \boldsymbol{\eta}_{2:k-1}^{\star}). \tag{67}$$

Equivalently to the source tracking filter derivation, the denominator in (65) can be factorized as

$$q(\mathbf{x}_{0:k}^{(i)} \mid \mathbf{z}_{1:k}, \boldsymbol{\eta}_{2:k}^{\star}) = q(\mathbf{x}_k^{(i)} \mid \mathbf{x}_{0:k-1}^{(i)}, \mathbf{z}_{1:k}, \boldsymbol{\eta}_{2:k}^{\star}) \, q(\mathbf{x}_{0:k-1}^{(i)} \mid \mathbf{z}_{1:k-1}, \boldsymbol{\eta}_{2:k-1}^{\star}), \tag{68}$$

where the first term on the R.H.S is simplified as $q(\mathbf{x}_k^{(i)} \mid \mathbf{x}_{0:k-1}^{(i)}, \mathbf{z}_{1:k}, \boldsymbol{\eta}_{2:k}^{\star}) = q(\mathbf{x}_k^{(i)} \mid \mathbf{x}_{k-1}^{(i)}, \mathbf{z}_{1:k}, \boldsymbol{\eta}_{2:k}^{\star})$ according to that the current state $\mathbf{x}_k^{(i)}$ given the measurement $\mathbf{z}_{1:k}$ and the predicted observations $\boldsymbol{\eta}_{2:k}^{\star}$ depends only on the previous state $\mathbf{x}_{k-1}^{(i)}$ and conditionally independent of all previous states $\mathbf{x}_{0:k-2}^{(i)}$. By substituting derived densities of the numerator and the denominator from (67) and (68) into (65), the particle weights can be rewritten as

$$w_k^{(i)} \propto w_{k-1}^{(i)} \frac{p(\mathbf{z}_k \mid \mathbf{x}_k^{(i)}) \, p(\boldsymbol{\eta}_k^{\star} \mid \mathbf{x}_k^{(i)}) \, p(\mathbf{x}_k^{(i)} \mid \mathbf{x}_{k-1}^{(i)})}{q(\mathbf{x}_k^{(i)} \mid \mathbf{x}_{k-1}^{(i)}, \mathbf{z}_{1:k}, \boldsymbol{\eta}_{2:k}^{\star})}. \tag{69}$$

References

[1] O. Alotaibi and B. L. Mark, "Bayesian transfer learning with particle filter for object tracking under asymmetric noise intensities," in *Proc. IEEE Conf. Control Technol. Appl. (CCTA)*, San Diego, CA, August 2025, pp. 464–469.

[2] Y. Bar-Shalom and L. Campo, "The effect of the common process noise on the two-sensor fused-track covariance," *IEEE Trans. Aerosp. Electron. Syst.*, vol. 22, pp. 803–805, Nov. 1986.

[3] J. A. Roecker and C. D. McGillem, "Comparison of two-sensor tracking methods based on state vector fusion and measurement fusion," *IEEE Trans. Aerosp. Electron. Syst.*, vol. 24, no. 4, pp. 447–449, Jul. 1988.

[4] H. R. Hashemipour, S. Roy, and A. J. Laub, "Decentralized structures for parallel Kalman filtering," *IEEE Trans. Autom. Control*, vol. 33, no. 1, pp. 88–94, 1988.

[5] S. J. Pan and Q. Yang, "A survey on transfer learning," *IEEE Trans. Knowl. Data Eng.*, vol. 22, no. 10, pp. 1345–1359, 2009.

[6] A. Karbalayghareh, X. Qian, and E. R. Dougherty, "Optimal Bayesian transfer learning," *IEEE Trans. Signal Process.*, vol. 66, no. 14, pp. 3724–3739, 2018.

[7] X. Wu, J. H. Manton, U. Aickelin, and J. Zhu, "A Bayesian approach to (online) transfer learning: Theory and algorithms," *Artif. Intell.*, vol. 324, p. 103991, 2023.

[8] C. Zhou, J. Zhang, J. Liu, C. Zhang, G. Shi, and J. Hu, "Bayesian transfer learning for object detection in optical remote sensing images," *IEEE Trans. Geosci. Remote Sens.*, vol. 58, no. 11, pp. 7705–7719, 2020.

[9] S. Zhao, T. Zhang, Y. S. Shmaliy, X. Luan, and F. Liu, "Bayesian transfer filtering using pseudo marginal measurement likelihood," *IEEE Trans. Cybern.*, vol. 55, no. 2, pp. 562–573, 2025.

[10] A. Karbalayghareh, X. Qian, and E. R. Dougherty, "Optimal Bayesian transfer regression," *IEEE Signal Process. Lett.*, vol. 25, no. 11, pp. 1655–1659, 2018.

[11] M. Papež and A. Quinn, "Transferring model structure in Bayesian transfer learning for Gaussian process regression," *Knowl. Base. Syst.*, vol. 251, p. 108875, 2022.

[12] Q. Wang, F. Chen, J. Yang, W. Xu, and M.-H. Yang, "Transferring visual prior for online object tracking," *IEEE Trans. Image Process.*, vol. 21, no. 7, pp. 3296–3305, 2012.

[13] X. He, X. Chen, X. Du, X. Wang, S. Xu, and J. Guan, "Maritime target radar detection and tracking via DTNet transfer learning using multi-frame images," *Remote Sens.*, vol. 17, no. 5, 2025.

[14] X. Chen, Y. Wang, L. Chen, and J. Ji, "Multi-vehicle cooperative target tracking with time-varying localization uncertainty via recursive variational Bayesian inference," *Sensors*, vol. 20, no. 22, 2020.

[15] Z. Wang, Y. Wang, Z. Wu, H. Ma, Z. Li, H. Qiu, and J. Li, "CMP: cooperative motion prediction with multi-agent communication," *IEEE Robot. Autom. Lett.*, vol. 10, no. 4, pp. 3876–3883, 2025.

[16] C. Foley and A. Quinn, "Fully probabilistic design for knowledge transfer in a pair of Kalman filters," *IEEE Signal Process. Lett.*, vol. 25, no. 4, pp. 487–490, 2017.

[17] M. Papež and A. Quinn, "Robust Bayesian transfer learning between Kalman filters," in *Proc. IEEE 29th Int. Workshop Mach. Learn. for Signal Process. (MLSP)*, Pittsburgh, PA, October 2019, pp. 1–6.

[18] ——, "Hierarchical Bayesian transfer learning between a pair of Kalman filters," in *Proc. 32nd Irish Signals Syst. Conf. (ISSC)*, Athlone, Ireland, June 2021, pp. 1–5.

[19] O. Skalský and J. Dokoupil, "Bayesian knowledge transfer for a Kalman fixed-lag interval smoother," *IEEE Control Syst. Lett.*, vol. 9, pp. 2037–2042, 2025.

[20] Y. Huang, T. Zhang, S. Zhao, and F. Liu, "Design of Bayesian transfer filter for systems with inequality constraints," in *Proc. 19th IEEE Int. Conf. Control Autom. (ICCA)*, Tallinn, Estonia, June 2025, pp. 797–802.

[21] O. Alotaibi and B. L. Mark, "Object tracking incorporating transfer learning into an unscented Kalman filter," in *Proc. 58th Annu. Conf. Inf. Sci. Syst. (CISS)*, Princeton, NJ, March 2024, pp. 1–6.

[22] D. Willner, C. B. Chang, and K. P. Dunn, "Kalman filter algorithms for a multi-sensor system," in *Proc. IEEE Conf. Decis. Control Including 15th Symp. Adapt. Processes*, Clearwater, FL, December 1976, pp. 570–574.

[23] R. Olfati-Saber, "Distributed Kalman filter with embedded consensus filters," in *Proc. 44th IEEE Conf. Decis. Control (CDC)*, Seville, Spain, December 2005, pp. 8179–8184.

[24] ——, "Distributed Kalman filtering for sensor networks," in *Proc. 46th IEEE Conf. Decis. Control (CDC)*, New Orleans, LA, December 2007, pp. 5492–5498.

[25] S. P. Talebi and S. Werner, "Distributed Kalman filtering: Consensus, diffusion, and mixed," in *Proc. IEEE Conf. Control Technol. Appl. (CCTA)*, Copenhagen, Denmark, August 2018, pp. 1126–1132.

[26] N. J. Gordon, D. J. Salmond, and A. F. M. Smith, "Novel approach to nonlinear/non-Gaussian Bayesian state estimation," *Proc. Inst. Elect. Eng. F (Radar Signal Process.)*, vol. 140, no. 2, pp. 107–113, April 1993.

[27] F. Gustafsson, F. Gunnarsson, N. Bergman, U. Forssell, J. Jansson, R. Karlsson, and P.-J. Nordlund, "Particle filters for positioning, navigation, and tracking," *IEEE Trans. Signal Process.*, vol. 50, no. 2, pp. 425–437, 2002.

[28] S. Julier, J. Uhlmann, and H. F. Durrant-Whyte, "A new method for the nonlinear transformation of means and covariances in filters and estimators," *IEEE Trans. Autom. Control*, vol. 45, no. 3, pp. 477–482, March 2000.

[29] I. Arasaratnam and S. Haykin, "Cubature Kalman filters," *IEEE Trans. Autom. Control*, vol. 54, no. 6, pp. 1254–1269, 2009.

[30] O. Alotaibi, B. L. Mark, and M. R. Fasihi, "Object tracking incorporating transfer learning into unscented and cubature Kalman filters," *arXiv:2408.07157*, 2024.

[31] O. Alotaibi and B. L. Mark, "Incorporating multi-source transfer learning into an unscented Kalman filter for object tracking," in *Proc. 59th Annu. Conf. Inf. Sci. Syst. (CISS)*, Baltimore, MD, March 2025, pp. 1–6.

[32] Y. Ho and R. Lee, "A Bayesian approach to problems in stochastic estimation and control," *IEEE Trans. Autom. Control*, vol. 9, no. 4, pp. 333–339, October 1964.

[33] J. S. Liu and R. Chen, "Sequential Monte Carlo methods for dynamic systems," *J. Amer. Statist. Assoc.*, vol. 93, no. 443, pp. 1032–1044, 1998.

[34] M. S. Arulampalam, S. Maskell, N. Gordon, and T. Clapp, "A tutorial on particle filters for online nonlinear/non-Gaussian Bayesian tracking," *IEEE Trans. Signal Process.*, vol. 50, no. 2, pp. 174–188, Feb. 2002.

[35] A. Doucet, S. Godsill, and C. Andrieu, "On sequential Monte Carlo sampling methods for Bayesian filtering," *Statist. Comput.*, vol. 10, no. 3, pp. 197–208, Jul. 2000.

[36] G. Kitagawa, "Monte Carlo filter and smoother for non-Gaussian nonlinear state space models," *J. Comput. Graph. Statist.*, vol. 5, no. 1, pp. 1–25, 1996.

[37] Y. Bar-Shalom, X. R. Li, and T. Kirubarajan, *Estimation with Applications to Tracking and Navigation: Theory Algorithms and Software*.   New York, NY: Wiley, 2001.